

Effective transport by 2D turbulence: Vortex-gas intermittency vs. Kraichnan-Leith-Batchelor theory

Julie Meunier¹ and Basile Gallet¹

¹*Université Paris-Saclay, CNRS, CEA, Service de Physique de l'Etat Condensé, 91191 Gif-sur-Yvette, France.*

The Kraichnan-Leith-Batchelor (KLB) inverse energy cascade is a hallmark of 2D turbulence, with its theoretical energy spectrum observed in both Direct Numerical Simulations (DNS) and laboratory experiments. Surprisingly, however, we show that the effective diffusivity of 2D turbulent flows significantly depart from the KLB scaling prediction. We illustrate this phenomenon based on a suite of DNS of 2D turbulent flows forced at intermediate wavenumber and damped by weak linear or quadratic drag. We derive alternate scaling predictions based on the emergence of intense, isolated vortices causing spatially intermittent frictional dissipation localized within the small vortex cores. The predictions quantitatively match DNS data. This study points to a universal large-scale organization of 2D turbulent flows in physical space, bridging standard 2D Navier-Stokes turbulence with large-scale geophysical turbulence.

Introduction.— Many turbulent flows are effectively described by two-dimensional (2D) equations as a result of small aspect ratio, global rotation or external magnetic field [1–10], in situations ranging from large-scale flows in oceans and planetary atmospheres [11–14], to plasma physics [15, 16], liquid-metal experiments [1, 17–19] and active matter systems [20, 21]. The phenomenology of 2D turbulence strongly departs from that of 3D turbulence. The conservation of both energy and enstrophy by 2D flows induces inverse energy transfers, from smaller to larger scales, together with forward enstrophy transfers, from larger to smaller scales. When energy is supplied by some forcing mechanism at wavenumber k_f and removed at large scales by some damping mechanism, the Kraichnan-Leith-Batchelor (KLB) scaling theory predicts the existence of an inverse energy cascade characterized by an energy spectrum proportional to $k^{-5/3}$, where k denotes wavenumber [22]. Just as for the standard (forward) energy cascade of 3D turbulence, the theory assumes local energy transfers within an ‘inertial’ range of wavenumbers devoid of forcing and dissipative effects.

The $k^{-5/3}$ energy spectrum has been observed in both laboratory experiments and Direct Numerical Simulations (DNS) [8, 17, 23–26], making the KLB theory standard textbook material [27, 28]. Beyond the sole energy spectrum, however, one is often interested in the large-scale organization of the flow and in its effective transport properties as it acts on a much larger-scale tracer distribution: given a large-scale background gradient of some passive tracer, what is the mean scalar flux induced by the 2D turbulent flow, or equivalently, what is the effective diffusivity of the turbulent flow? Beyond their implications for oceanic and atmospheric flows (see *discussion* section), these fundamental questions constitute a test-case to evaluate the completeness and robustness of the KLB theory.

In the following we thus report a numerical and theoretical study aimed at characterizing the effective diffusivity of 2D turbulent flows. The DNS flow is driven at a

scale much smaller than the domain size. It is damped by a drag force, either linear or quadratic in velocity. Linear drag is motivated by the Hartmann friction of quasi-2D magnetohydrodynamic flows [17] and the Ekman friction of quasi-2D rapidly rotating flows [11–13].

With the goal of better modeling the turbulent drag force on the roughness elements of the Earth surface and Ocean floor, atmospheric and Ocean models often resort to a quadratic drag force instead, proportional to the local velocity squared [29–31].

Based on the DNS data, we report the following surprising observation: although power-law fits to the numerical spectra yield exponents close to $-5/3$, in line with the KLB theory and previous studies [23–26], we show that the KLB theory fails at predicting the effective diffusivity of the flow. This is because the KLB phenomenology only describes the magnitude of the Fourier amplitudes in spectral space, leaving aside the phase information. However, in line with previous studies, we observe that the flow organizes at large scale into a gas of coherent vortices [32–35]. Such coherent structures correspond to precise phase relations in spectral space that are not captured by the KLB theory. Also suggestive of the importance of coherent vortices is the fact that a successful vortex-based scaling theory for freely evolving 2D turbulence has been around for decades [36, 37]. Finally, Chang & Held noticed that the predictions of the KLB theory are not satisfied by the quasi-2D ‘baroclinic’ turbulence arising in models of large-scale ocean and atmospheric flows with quadratic drag [31]. In this context, the crucial role of large-scale vortices [38] is the starting point of a scaling theory put forward by Gallet & Ferrari ([39], GF in the following), but a connection to standard 2D Navier-Stokes turbulence has so far remained elusive. The goal of this Letter is to establish this connection through the development of a quantitative vortex-based theory for the eddy diffusivity of 2D Navier-Stokes turbulence with drag.

Forced 2D turbulence with drag.— We consider a two-

dimensional incompressible flow $\mathbf{u} = (u, v) = (-\psi_y, \psi_x)$ inside a doubly periodic domain $[0, 2\pi L]^2$. The flow is driven at small scale by the curl of a body-force, $f(x, y, t)$, peaked around a wavenumber k_f . The governing equation for the vorticity $\zeta = \Delta\psi$ reads

$$\partial_t \zeta + J(\psi, \zeta) = -\mathcal{D}(\psi) + f(x, y, t) - \nu \Delta^4 \zeta, \quad (1)$$

Where $J(g, h) = g_x h_y - g_y h_x$ denotes the Jacobian operator and ν denotes the hyperviscosity coefficient. The drag term $\mathcal{D}(\psi)$ corresponds to (the curl of) either a linear or a quadratic drag force. Denoting as κ (resp. μ) the linear (resp. quadratic) drag coefficient, the drag term reads:

$$\mathcal{D}(\psi) = \begin{cases} \kappa \Delta \psi & \text{linear drag} \\ \mu \left[(|\nabla \psi| \psi_x)_x + (|\nabla \psi| \psi_y)_y \right] & \text{quadratic drag.} \end{cases}$$

We consider two small-scale forcing protocols. Following the most widely adopted setup in the literature [24–26, 30, 40], in a first suite of numerical runs $f(x, y, t)$ is white-noise-in-time isotropic forcing inside a narrow band of wavenumbers centered around k_f . In a second suite of numerical runs $f(y)$ is steady ‘Kolmogorov’ forcing proportional to $\cos(k_f y)$ [41–43]. For the former forcing the mean energy injection rate per unit mass of fluid ϵ is a control parameter of the system, while for the latter forcing ϵ is an emergent parameter. Regardless, we use ϵ to characterize the strength of the forcing in both cases.

To diagnose the effective diffusivity of the flow, we consider the advection of a passive tracer subject to a uniform background gradient [30, 40]. The tracer evolution equation being linear, without loss of generality we set the large-scale gradient to minus one and denote as $\tau(x, y, t)$ the doubly periodic departure from the background gradient. The evolution equation for τ then reads

$$\partial_t \tau + J(\psi, \tau) = \psi_x - \nu \Delta^4 \tau, \quad (2)$$

where we employ the same hyperdiffusion coefficient as in (1) (see Supplemental Material for a Table of all parameter values). We perform DNS of equations (1) and (2) using a pseudo-spectral solver running on GPU with resolution up to 8192×8192 . Once the system has reached a statistically steady state, we extract ϵ together with the effective diffusivity of the flow. Because the background tracer gradient is set to -1 , the effective diffusivity equals the tracer flux, $D = \langle \psi_x \tau \rangle$, where the angular brackets denote time and space average. The energy spectra, provided as End Matter, are very similar to the ones reported in previous studies [23–26], with best-fit exponents close to $-5/3$ for $k < k_f$. We focus on the large-domain small-hyperviscosity limit where D is independent of both L and ν (as assessed by running DNS with various L and ν). We illustrate this regime in Fig. 1, where we show snapshots of the tracer departure field τ , of the vorticity ζ and of the Okubo-Weiss parameter $Q = \psi_{xy}^2 - \psi_{xx}\psi_{yy}$ [44, 45].

Because the inverse energy transfers are arrested by the drag term at a scale smaller than L , preventing the formation of a large-scale condensate, the effective diffusivity D depends only on the injection wavenumber k_f , the energy input rate ϵ and the drag coefficient κ or μ . In dimensionless form, we thus seek the dependence of the dimensionless diffusivity $\hat{D} = D\epsilon^{-1/3}k_f^{4/3}$ on the dimensionless drag coefficient $\hat{\kappa} = \kappa\epsilon^{-1/3}k_f^{-2/3}$ or $\hat{\mu} = \mu/k_f$.

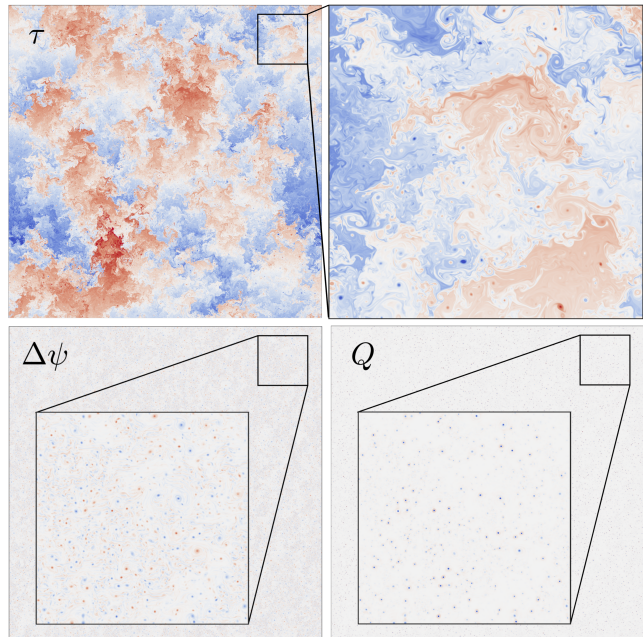


FIG. 1: Snapshots of the passive tracer departure field τ (upper panels), of the vorticity field $\Delta\psi$ (bottom left) and of the Okubo-Weiss parameter Q (bottom right) for a typical 4096×4096 run with quadratic drag $\mu/k_f = 5 \times 10^{-4}$ and Kolmogorov forcing at $k_f L = 400$ (positive values in red, negative values in blue, zero is white).

Diffusivity according to KLB.— As discussed in Refs. [30, 40], the KLB theory leads to compact predictions for the effective diffusivity. The assumption of an inertial range with local inverse energy transfers implies that large-scale quantities depend on the energy flux ϵ and on the friction coefficient arresting the inverse energy cascade, while they are independent of the small forcing scale k_f^{-1} . Dimensional analysis then yields $D \sim \epsilon/\kappa^2$ for linear drag and $D \sim \epsilon^{1/3}/\mu^{4/3}$ for quadratic drag, which we recast in terms of the dimensionless quantities as [30]:

$$\hat{D} \sim \hat{\kappa}^{-2}, \quad \hat{D} \sim \hat{\mu}^{-4/3}, \quad (3)$$

for linear and quadratic drag, respectively.

We compare these predictions to the DNS data in Fig. 2. Surprisingly, the numerical data depart from the KLB predictions (3) for both linear and quadratic drag, as clearly illustrated by the compensated plots in the insets. In contrast with the KLB theory, the diffusivity

of the turbulent flow clearly retains some dependence on the small injection scale k_f^{-1} .

Diffusivity according to vortex-gas dynamics.— A striking flow feature in physical space is the emergence of coherent vortices, as highlighted by the snapshot of Q in Fig. 1.

With the goal of including them in a scaling theory, we model the coherent vortices using an idealized vortex-gas framework, in a similar fashion to GF [39, 46]. We consider a population of identical vortices of circulation $\pm\Gamma$ and core radius r , the typical vorticity within the vortex cores being $\zeta_{\text{core}} \sim \Gamma/r^2$. The vortex-gas is dilute, with a typical inter-vortex distance $\ell \gg r$. The vortices wander around as a result of mutual induction with a typical velocity $V \sim \Gamma/\ell$, the latter being also the typical large-scale velocity in the inter-vortex region between vortices. Assuming that the transport properties of a single dipole of oppositely signed vortices correctly reflect transport within the vortex gas, GF show that:

$$D \sim \ell V \sim \Gamma. \quad (4)$$

In the inter-vortex region, energy injection and inverse transfers proceed following the standard KLB phenomenology [35, 47], leading to the following estimate for the large-scale velocity V at the large inter-vortex distance ℓ :

$$V \sim (\epsilon \ell)^{1/3}. \quad (5)$$

Combining this relation with (4) leads to expressions for V and ℓ in terms of D and ϵ :

$$V \sim D^{1/4} \epsilon^{1/4}, \quad \ell \sim D^{3/4} \epsilon^{-1/4}. \quad (6)$$

The last two scaling arguments are based, respectively, on the energy and enstrophy power integrals. The spatially intermittent nature of frictional damping comes into play through the energy power integral. Hyperviscous energy dissipation being negligible, the energy power integral reads $\epsilon = \kappa \langle \mathbf{u}^2 \rangle$ for linear drag and $\epsilon = \mu \langle |\mathbf{u}|^3 \rangle$ for quadratic drag. Following GF, we estimate the second and third moments of the vortex-gas velocity field by considering a single isolated Rankine vortex of core radius r and circulation Γ located at the center of a disk-shaped domain of radius ℓ . Computing the space average of \mathbf{u}^2 and $|\mathbf{u}|^3$ over the disk-shaped domain for this idealized velocity field yields $\langle \mathbf{u}^2 \rangle \sim V^2 \log(\ell/r)$ and $\langle |\mathbf{u}|^3 \rangle \sim V^3 \ell/r$, which we substitute into the energy power integral to obtain:

$$\epsilon \sim \kappa V^2 \log\left(\frac{\ell}{r}\right), \quad \epsilon \sim \mu V^3 \frac{\ell}{r}, \quad (7)$$

for linear and quadratic drag, respectively. Finally, an estimate for the core radius r can be deduced from the

enstrophy power integral. Following the vortex-gas description of freely evolving turbulence in Refs. [37, 48], we adopt the picture of an isolated vortex being reinforced through continuous mergers with smaller intense vorticity structures [32]. This process leads to filamentation and enstrophy dissipation in the vicinity of the vortex core, a region of both strong vorticity and strong strain. The flux of enstrophy to small dissipative scales through this process is the product of the typical enstrophy in this region, ζ_{core}^2 , with the local strain rate $\Gamma/r^2 \sim \zeta_{\text{core}}$. We thus estimate the enstrophy flux as ζ_{core}^3 within the near-core regions, that is, over a fraction r^2/ℓ^2 of the domain. The contribution of the near-core regions to the space-averaged enstrophy dissipation rate is thus estimated as $\zeta_{\text{core}}^3 r^2/\ell^2$. Demanding that the latter be less than or equal to the enstrophy injection rate $k_f^2 \epsilon$ leads to the following inequality for the vortex core radius:

$$r \lesssim \frac{k_f \epsilon^{1/2} \ell}{\zeta_{\text{core}}^{3/2}}. \quad (8)$$

As discussed in Ref. [37], isolated vortices within the vortex gas reinforce and expand through mergers, conserving energy and core vorticity, while dissipating enstrophy. They can do so as long as enstrophy dissipation by the mergers is smaller than enstrophy injection by the forcing. In the equilibrated state, we thus expect inequality (8) to be saturated. We thus replace the inequality (8) with an equality, before combining the resulting relation with (4) and (6), together with $\zeta_{\text{core}} \sim \Gamma/r^2 \sim D/r^2$. This leads to the following estimate for the dimensionless core radius:

$$k_f r \sim \hat{D}^{3/8}. \quad (9)$$

Starting from the energy power integral (7), one finally substitutes the estimates (6) and (9) for V , ℓ and r . This leads to the following scaling predictions for the eddy diffusivity of the flow in terms of the dimensionless drag coefficient:

$$\hat{D} \log^2 \hat{D} \sim \hat{\kappa}^{-2}, \quad \hat{D} \sim \hat{\mu}^{-8/9}, \quad (10)$$

for linear and quadratic drag, respectively. In contrast with the KLB scaling argument, reverting to dimensional quantities indicates that the predicted eddy diffusivity (10) explicitly involves the forcing scale: $D \log^2 [D \epsilon^{-1/3} k_f^{4/3}] \sim \epsilon/\kappa^2$ or $D \sim \epsilon^{1/3} k_f^{-4/9} \mu^{-8/9}$. As shown in Fig. 2, the predictions (10) capture the numerical data with excellent accuracy in the low-drag regime, for both types of drag and both forcing protocols.

Discussion: connection to baroclinic turbulence.— Interestingly, the present scaling theory sheds new light on traditional approaches to parameterize ‘baroclinic’ turbulence in oceans and atmospheres [31, 40, 49, 50]. Baroclinic turbulence is a form of quasi-2D turbulence driven

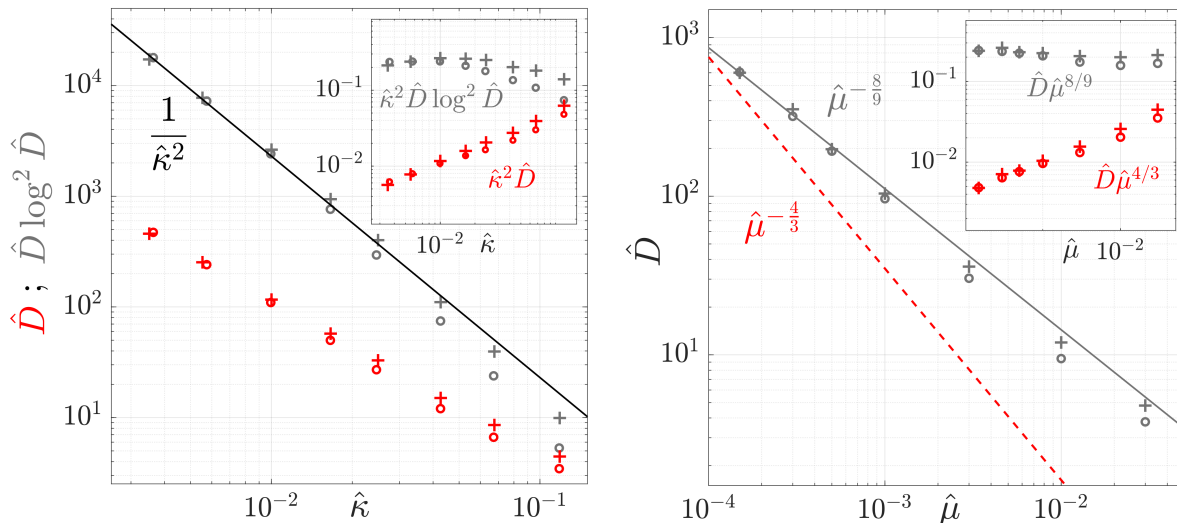


FIG. 2: Dimensionless effective diffusivity \hat{D} as a function of the dimensionless drag coefficient. Symbols are DNS data (+: white-noise forcing ; \circ : Kolmogorov forcing). In the left-hand panel we plot both \hat{D} and $\hat{D} \log^2 \hat{D}$ as functions of $\hat{\kappa}$ to test the KLB prediction and the vortex-gas prediction, respectively. In the right-hand panel we plot the effective diffusivity as a function of the quadratic drag coefficient, together with the KLB prediction (dashed line) and the vortex-gas prediction (solid line). Inset: compensated plots using both the KLB theory (red) and the present theory (gray).

by an instability mechanism that injects kinetic energy around a small spatial scale λ (the Rossby deformation radius [11–13, 51]). The 2D velocity field is coupled to a temperature field τ , which has dimensions of a streamfunction. The latter is subject to a background meridional gradient denoted as U in this context. The source of kinetic energy in baroclinic turbulence is the meridional transport of heat, hence a direct proportionality relation between the mean meridional heat flux and the mean kinetic energy dissipation rate of the flow, $\epsilon = DU^2/\lambda^2$. The sink of kinetic energy is linear or quadratic drag. The dimensional control parameters are U , λ and the drag coefficient in this context, and scaling theories aim at relating the dimensionless diffusivity $D_* = D/(U\lambda)$ to the dimensionless drag coefficient $\kappa_* = \kappa\lambda/U$ or $\mu_* = \mu\lambda$. Although the equations governing baroclinic turbulence depart from the standard 2D Navier-Stokes equation, the traditional approach to deriving a scaling theory is based on a parallel between the two systems: one assumes that the forcing wavenumber is $k_f \sim \lambda^{-1}$ and combines the relation $\epsilon = DU^2/\lambda^2$ with estimates for D based on the phenomenology of 2D turbulence. However, combining this relation with the KLB prediction (3) for quadratic drag leads to $D_* \sim 1/\mu_*^2$, a prediction clearly invalidated by DNS of baroclinic turbulence [31, 39, 46, 52] (a similar failure arises for linear drag). In parallel, GF and later Hadjerci & Gallet ([46], HG in the following) designed a purely vortex-based theory that captures the behavior of D_* with drag κ_* or μ_* with excellent accuracy. The puzzle remained why baroclinic turbulence would behave so differently from standard 2D Navier-Stokes turbulence.

The present study solves this puzzle by insisting that emergent coherent vortices are, in fact, a crucial ingredient of standard 2D Navier-Stokes turbulence too. When the relations $\epsilon = DU^2/\lambda^2$ and $k_f \sim \lambda^{-1}$ are combined with the new scaling predictions (10) for the 2D Navier-Stokes diffusivity, one recovers the successful predictions of HG for the dependence of D_* on κ_* or μ_* .

Conclusion.— We have reported a suite of DNS of 2D Navier-Stokes turbulence with drag, focussing of the effective diffusivity of the flow. By reaching lower drag than previous studies [30, 40], we identified clear departures from the KLB scaling predictions. We thus proposed an alternate scaling theory that takes into account the emergent coherent vortices that populate 2D turbulent flows. Coherent vortices derail the KLB scaling predictions because they induce localized frictional dissipation within the small vortex cores. To some extent, the present scaling predictions thus result from a strong form of intermittency, a term initially referring to the strongly inhomogeneous spatial distribution of the energy dissipation rate [28, 53–55]. In standard 3D turbulent flows, intermittency effects intensify as the cascade proceeds to smaller scales. They are essential for understanding the fine-scale properties, while having minimal impact on large-scale properties like effective diffusivity, flow kinetic energy, and the integral scale, which align with the Kolmogorov-Obukhov theory. Conversely, in 2D turbulent flows with drag, intermittency effects increase as the cascade proceeds from small to large scales, significantly influencing large-scale quantities and causing the KLB theory to fail in predicting the effective diffusivity.

End matter: Energy spectra

In Fig.3 we plot the energy spectra extracted from DNS performed with white-noise forcing and both types of drag, together with a $k^{-5/3}$ eyeguide. As expected, the spectra are very similar to the ones reported in previous numerical studies with white-noise forcing and (linear) drag, see e.g. Ref. [25]. To extract a spectral slope in the inverse cascade range, we first introduce an energy-containing wavenumber $k_L^2 = \langle \mathbf{u}^2 \rangle / \langle \psi^2 \rangle$, before performing a power-law fit to each spectrum over the range $k \in [k_L, k_f]$. The resulting power-law exponent α is compared to the KLB value $-5/3$ in the inset of each panel, where we plot the ratio $\delta = \alpha / (-5/3)$. The best-fit exponent α is within 15% percents of the theoretical value $-5/3$ at low drag.

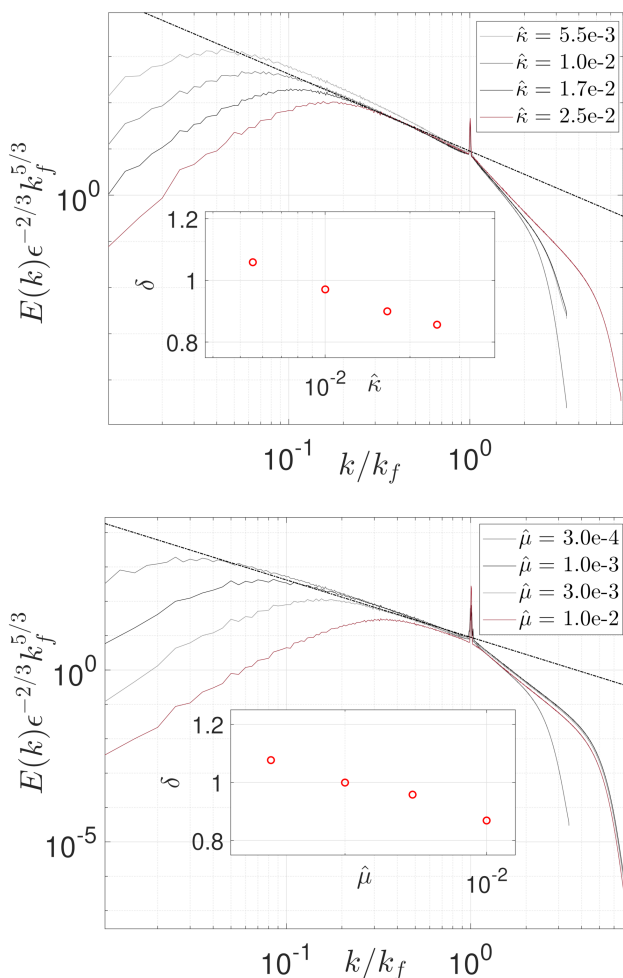


FIG. 3: Energy spectra from sample simulations with linear (top) and quadratic (bottom) drag, driven by white-noise-in-time forcing. The spectra are non-dimensionalized using ϵ and k_f . The inset displays the ratio δ of the best-fit exponent α to the KLB prediction $-5/3$.

- [1] J. Sommeria and R. Moreau. Why, how and when, mhd turbulence becomes two-dimensional. *Journal of Fluid Mechanics*, 118:507–518, 1982.
- [2] P. A. Davidson. *Turbulence in rotating, stratified and electrically conducting fluids*. Cambridge University Press, 2013.
- [3] E. Deusebio, G. Boffetta, E. Lindborg, and S. Musacchio. Dimensional transition in rotating turbulence. *Physical Review E*, 90(2):023005, 2014.
- [4] B. Gallet and C. R. Doering. Exact two-dimensionalization of low-magnetic-reynolds-number flows subject to a strong magnetic field. *Journal of Fluid Mechanics*, 773:154–177, 2015.
- [5] B. Gallet. Exact two-dimensionalization of rapidly rotating large-reynolds-number flows. *Journal of Fluid Mechanics*, 783:412–447, 2015.
- [6] S. J. Benavides and A. Alexakis. Critical transitions in thin layer turbulence. *Journal of Fluid Mechanics*, 822:364–385, 2017.
- [7] K. Seshasayanan and A. Alexakis. Condensates in rotating turbulent flows. *Journal of Fluid Mechanics*, 841:434–462, 2018.
- [8] A. Alexakis and L. Biferale. Cascades and transitions in turbulent flows. *Physics Reports*, 767-769:1–101, 2018. Cascades and transitions in turbulent flows.
- [9] A. van Kan and A. Alexakis. Condensates in thin-layer turbulence. *Journal of Fluid Mechanics*, 864:490–518, 2019.
- [10] K. Seshasayanan and B. Gallet. Onset of three-dimensionality in rapidly rotating turbulent flows. *Journal of Fluid Mechanics*, 901:R5, 2020.
- [11] R. Salmon. *Lectures on geophysical fluid dynamics*. Oxford University Press, USA, 1998.
- [12] J. Pedlosky. *Geophysical fluid dynamics*. Springer Science & Business Media, 2013.
- [13] G. K. Vallis. *Atmospheric and oceanic fluid dynamics*. Cambridge University Press, 2017.
- [14] L. Miller, B. Deremble, and A. Venaille. Gyre turbulence: Anomalous dissipation in a two-dimensional ocean model. *Physical Review Fluids*, 9(5):L051801, 2024.
- [15] C. F. Driscoll and K. S. Fine. Experiments on vortex dynamics in pure electron plasmas. *Physics of Fluids B: Plasma Physics*, 2(6):1359–1366, 1990.
- [16] C. F. Driscoll, D. Z. Jin, D. A. Schecter, and D. H. E. Dubin. Vortex dynamics of 2d electron plasmas. *Physica C: Superconductivity*, 369(1-4):21–27, 2002.
- [17] J. Sommeria. Experimental study of the two-dimensional inverse energy cascade in a square box. *Journal of fluid mechanics*, 170:139–168, 1986.
- [18] B. Gallet, J. Hœrault, C. Laroche, F. Pétrélis, and S. Fauve. Reversals of a large-scale field generated over a turbulent background. *Geophysical & Astrophysical Fluid Dynamics*, 106(4-5):468–492, 2012.
- [19] G. Michel, J. Hœrault, F. Pétrélis, and S. Fauve. Bifurcations of a large-scale circulation in a quasi-bidimensional turbulent flow. *Europhysics Letters*, 115(6):64004, 2016.
- [20] B. Martínez-Prat, R. Alert, J. Ignés-Mullol F. Meng, J-F Joanny, J. Casademunt, R. Golestanian, and F. Sagués. Scaling regimes of active turbulence with external dissipation. *Physical Review X*, 11(3):031065, 2021.
- [21] D. Bárdfalvy, and C. Nardini V. Škultéty, A. Morozov,

- and J. Stenhammar. Collective motion in a sheet of microswimmers. *Communications Physics*, 7(1):93, 2024.
- [22] R. H. Kraichnan. Inertial ranges in two-dimensional turbulence. *Physics of fluids*, 10(7):1417, 1967.
- [23] Guido Boffetta, Antonio Celani, and Massimo Vergasola. Inverse energy cascade in two-dimensional turbulence: Deviations from gaussian behavior. *Physical Review E*, 61(1):R29, 2000.
- [24] S. Chen, R. E. Ecke, G. L. Eyink, M. Rivera, M. Wan, and Z. Xiao. Physical mechanism of the two-dimensional inverse energy cascade. *Physical review letters*, 96(8):084502, 2006.
- [25] G. Boffetta and S. Musacchio. Evidence for the double cascade scenario in two-dimensional turbulence. *Physical Review E—Statistical, Nonlinear and Soft Matter Physics*, 82(1):016307, 2010.
- [26] G. Boffetta and R. E. Ecke. Two-dimensional turbulence. *Annual review of fluid mechanics*, 44:427–451, 2012.
- [27] M. Lesieur. Introduction to turbulence in fluid mechanics. *Turbulence in Fluids: Fourth Revised and Enlarged Edition*, pages 1–23, 2008.
- [28] U. Frisch. *Turbulence: the legacy of AN Kolmogorov*. Cambridge university press, 1995.
- [29] J. R. Holton and G. J. Hakim. *An introduction to dynamic meteorology*, volume 88. Academic press, 2013.
- [30] N. Gryanik, I. M. Held, K. S. Smith, and G. K. Vallis. The effects of quadratic drag on the inverse cascade of two-dimensional turbulence. *Physics of Fluids*, 16(1):73–78, 01 2004.
- [31] C. Y. Chang and I. M. Held. The control of surface friction on the scales of baroclinic eddies in a homogeneous quasigeostrophic two-layer model. *Journal of the Atmospheric Sciences*, 76(6):1627 – 1643, 2019.
- [32] V. Borue. Inverse energy cascade in stationary two-dimensional homogeneous turbulence. *Physical review letters*, 72(10):1475, 1994.
- [33] S. Danilov and D. Gurarie. Nonuniversal features of forced two-dimensional turbulence in the energy range. *Physical Review E*, 63(2):020203, 2001.
- [34] R. K. Scott. Nonrobustness of the two-dimensional turbulent inverse cascade. *Physical Review E—Statistical, Nonlinear and Soft Matter Physics*, 75(4):046301, 2007.
- [35] B. H. Burgess, D. G. Dritschel, and R. K. Scott. Vortex scaling ranges in two-dimensional turbulence. *Physics of Fluids*, 29(11), 2017.
- [36] J. C. McWilliams. The vortices of two-dimensional turbulence. *Journal of Fluid mechanics*, 219:361–385, 1990.
- [37] G. F. Carnevale, J. C. McWilliams, Y. Pomeau, J. B. Weiss, and W. R. Young. Evolution of vortex statistics in two-dimensional turbulence. *Phys. Rev. Lett.*, 66:2735–2737, May 1991.
- [38] A. F. Thompson and W. R. Young. Scaling baroclinic eddy fluxes: Vortices and energy balance. *Journal of physical oceanography*, 36(4):720–738, 2006.
- [39] B. Gallet and R. Ferrari. The vortex gas scaling regime of baroclinic turbulence. *Proceedings of the National Academy of Sciences*, 117(9):4491–4497, 2020.
- [40] K. S. Smith, G. Boccaletti, C. C. Henning, I. Marinov, C. Y. Tam, I. M. Held, and G. K. Vallis. Turbulent diffusion in the geostrophic inverse cascade. *Journal of Fluid Mechanics*, 469:13–48, 2002.
- [41] J. M. Burgess, C. Bizon, W. D. McCormick, J. B. Swift, and H. L. Swinney. Instability of the kolmogorov flow in a soap film. *Physical Review E*, 60(1):715, 1999.
- [42] M. Rivera and X-L Wu. External dissipation in driven two-dimensional turbulence. *Physical review letters*, 85(5):976, 2000.
- [43] Y. K. Tsang and W. R. Young. Forced-dissipative two-dimensional turbulence: A scaling regime controlled by drag. *Phys. Rev. E*, 79:045308, Apr 2009.
- [44] A. Okubo. Horizontal dispersion of floatable particles in the vicinity of velocity singularities such as convergences. In *Deep sea research and oceanographic abstracts*, volume 17, pages 445–454. Elsevier, 1970.
- [45] J. Weiss. The dynamics of enstrophy transfer in two-dimensional hydrodynamics. *Physica D: Nonlinear Phenomena*, 48(2-3):273–294, 1991.
- [46] G. Hadjerci and B. Gallet. Vortex core radius in baroclinic turbulence: Implications for scaling predictions. *Phys. Rev. Fluids*, 8:094501, Sep 2023.
- [47] J. Wang, J. Sesterhenn, and W. C. Müller. Coherent structure detection and the inverse cascade mechanism in two-dimensional navier–stokes turbulence. *Journal of Fluid Mechanics*, 963:A28, 2023.
- [48] J. B. Weiss. Punctuated hamiltonian models of structured turbulence. *Semi-Analytic Methods for the Navier–Stokes Equations (Montreal, Canada, 1995)*(ed. K. Coughlin). CRM Proc. Lecture Notes, 20:109–119, 1999.
- [49] I. M. Held. The macroturbulence of the troposphere. *Tellus A*, 51(1):59–70, 1999.
- [50] V. D. Larichev and I. M. Held. Eddy amplitudes and fluxes in a homogeneous model of fully developed baroclinic instability. *Journal of Physical Oceanography*, 25(10):2285 – 2297, 1995.
- [51] B. Gallet, B. Miquel, G. Hadjerci, K. J. Burns, G. R. Flierl, and R. Ferrari. Transport and emergent stratification in the equilibrated eady model: the vortex-gas scaling regime. *Journal of Fluid Mechanics*, 948:A31, 2022.
- [52] G. Hadjerci and B. Gallet. Two-layer baroclinic turbulence with arbitrary layer depths. *Physical Review Fluids*, 9(5):L051802, 2024.
- [53] A. N. Kolmogorov. A refinement of previous hypotheses concerning the local structure of turbulence in a viscous incompressible fluid at high reynolds number. *Journal of Fluid Mechanics*, 13(1):82–85, 1962.
- [54] B. Pearson and B. Fox-Kemper. Log-normal turbulence dissipation in global ocean models. *Physical review letters*, 120(9):094501, 2018.
- [55] B. Dubrulle. Beyond kolmogorov cascades. *Journal of Fluid Mechanics*, 867:P1, 2019.